Gold Nanoclusters

DOI: 10.1002/anie.201100299

Insulin-Directed Synthesis of Fluorescent Gold Nanoclusters: Preservation of Insulin Bioactivity and Versatility in Cell Imaging

Chien-Liang Liu, Hung-Tsung Wu, Yi-Hsuan Hsiao, Chih-Wei Lai, Chun-Wei Shih, Yung-Kang Peng, Kuo-Chun Tang, Hsing-Wei Chang, Yun-Chen Chien, Jong-Kai Hsiao, Juei-Tang Cheng, and Pi-Tai Chou**

Fluorescent nanomaterials have received great attention and have been intensively studied, because of their unique optical and photophysical properties, as replacements for conventional organic dyes in optical cell imaging.[1] Although semiconductor quantum dots show promising signals in biomedical imaging,[2] their high inherent cytotoxicity and self-aggregation inside living cells[3] fatally limit pragmatic biomedical applications. Fluorescent nanoclusters (NCs), in contrast, exhibit superior properties such as low toxicity and high biocompatibility. Among the various NCs, much effort has been dedicated to the study of fluorescent Au NCs.[4,5] Au NCs carry quantum-mechanical properties when their sizes are comparable to or smaller than the Fermi wavelength (ca. 1 nm) of conductive electrons.[6]

The fluorescent Au NCs, with their ultrafine size, do not disturb the biological functions of the labeled bioentities; therefore, there is great potential to develop Au NCs as a new luminescent label.[7] For example, Lin et al. successfully used water-soluble fluorescent Au NCs capped with dihydrolipoic acid (AuNC@DHLA) and modified with polyethylene glycol (PEG), bovine serum albumin (BSA), and streptavidin for cell bioimaging.[8] Compared with organic-monolayer-protected Au NCs, the usage of proteins as a green-chemical reducing and stabilizing agent is advantageous because their complex 3D structures can withstand a wide range of pH conditions.[9] Accordingly, Au NC synthesis with BSA[10] and lysozyme[11] has been reported and applied to several devices, such as nanosensors of Hg^{2+}, CN^-, and H_2O_2.[12] Very recently, through the conjugation of BSA–Au NCs to folic acid, target-specific detection of cancer-cell imaging has been demonstrated.[9a] Also, BSA–Au NCs have been applied in MDA-MB-45 and HeLa tumor xenograft model imaging.[13] Nevertheless, up to this stage, there has been a lack of reports on bioactive protein-directed fluorescent Au NCs that can still preserve their own biological role. Conversely, using Au nanoparticles encapsulated in certain enzymes, several reports claimed significant changes of enzymatic functionality.[14]

The goal of this project is thus to search for a bioactive protein to exploit as a template to direct the growth of fluorescent Au NCs. The resulting protein–Au NC nanocomposites are able to retain bioactivity, so that the associated biological role can be pursued by various imaging techniques. Among a number of proteins of vital importance, insulin is of prime interest. Insulin is a polypeptide hormone comprising only 51 amino acids. Its function primarily lies in the regulation of insulin-responsive tissues and it is also directly/indirectly related to many diseases, including diabetes, Alzheimer's disease,[15] obesity,[16] and aging.[17] Its signaling pathway controls the growth of an organism, and hence exerts a profound influence on metabolism and reproduction.

Herein, we report for the first time the synthesis of fluorescent Au NCs by using insulin as a template. The resulting insulin–Au NCs exhibit intense red fluorescence maximized at 670 nm and, more importantly, retain their bioactivity and biocompatibility. Several key experiments have been performed in vitro and/or in vivo to assess their viability and versatility.

Detailed synthetic procedures are elaborated in the Supporting Information. In brief, by mixing insulin and $HAuCl_4$ in Na_3PO_4 buffer by continuously stirring at 4°C for 12 h, reddish luminescent insulin–Au NCs were readily prepared. The crude product was then purified by centrifugal filtration (4000 *g*) for 30 min with a cutoff of 5 kDa to obtain the insulin–Au NCs for subsequent applications. The absorption and photoluminescence emission spectra of insulin–Au NCs are shown in Figure 1. The emission quantum yield Φ_f was determined to be 0.07, with observed lifetimes fitted to be 439 ns (4%) and 2041 ns (96%).[11]

The inset of Figure 1 displays a high-resolution transmission electron microscopy (HRTEM) image of insulin–Au NCs. From the respective histograms, the as-prepared insulin–Au NCs revealed a spherical shape and good size uniformity (for size distribution, see Figure S1 in the Supporting Information). The diameters of insulin–Au NCs, upon averaging over 100 particles, were calculated to be (0.92 ± 0.03) nm (mainly for Au NCs). The hydrodynamic radii of

[*] C.-L. Liu, Y.-H. Hsiao, Dr. C.-W. Lai, C.-W. Shih, Y.-K. Peng, Dr. K.-C. Tang, H.-W. Chang, Prof. P.-T. Chou
Department of Chemistry, National Taiwan University
1, Section 4, Roosevelt Road, Taipei 10617 (Taiwan)
Fax: (+886) 2-369-5208
E-mail: chop@ntu.edu.tw
H.-T. Wu, Prof. J.-T. Cheng
Department of Medical Research, Chi-Mei Medical Center
Yong Kang City, Tainan County 73101 (Taiwan)
E-mail: m980103@mail.chimei.org.tw
Prof. J.-K. Hsiao
Department of Medical Imaging, Buddhist Tzu-Chi General Hospital Taipei Branch (Taiwan)
Y.-C. Chien
Taipei First Girls' High School, Taipei 10045 (Taiwan)

Supporting information for this article is available on the WWW under http://dx.doi.org/10.1002/anie.201100299.

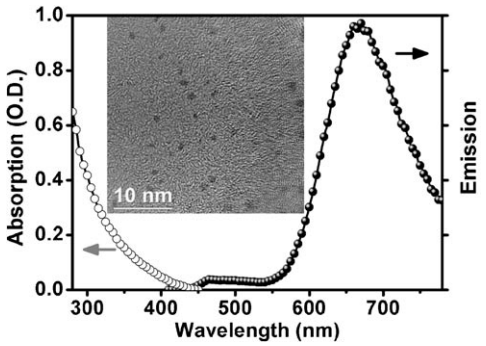

Figure 1. Absorption and emission spectra of aqueous solutions of insulin–Au NCs. The excitation wavelength is at 400 nm. Inset: Representative HRTEM image.

the insulin and insulin–Au NCs were also measured by dynamic light scattering, which gave diameters of (2.5 ± 0.7) and (3.5 ± 0.4) nm, respectively (see Figure S2 in the Supporting Information). Thermogravimetric analysis (TGA) of insulin–Au NC powder in air shows a weight loss of about 80% upon heating above 470 °C (see Figure S2c). Verification of Au composition was provided by energy-dispersive X-ray (EDX) spectroscopy of insulin–Au NCs (see Figure S3a in the Supporting Information). The in-depth chemical state of insulin–Au NCs was determined by X-ray photoelectron spectroscopy (XPS; see Figure S3b). The best fit of the data indicated that insulin–Au NCs consisted of approximately 24.3% Au^I and complementary metallic Au. The results are consistent with a previous study of thiol-protected Au NCs, which concluded the existence of a small amount of Au^I on the surface to help stabilize the Au NCs.[10]

We then made attempts to measure the mass of the as-prepared insulin–Au NCs. Interestingly, no Au attached to the insulin was detected in mass spectrometry, as evidenced by the lack of any mass peak larger than that of the parent insulin. This result is in sharp contrast to that for BSA–Au NCs, for which clear mass peaks of Au NCs associated with BSA could be observed. We then carefully examined the associated Au NC fragments in the mass spectra and again failed to resolve the related mass peaks. As for the BSA–Au NCs, it has been well established that the encapsulation of Au NCs occurs mainly through the Au–S bond, where 35 cysteine (Cys) residues act as capping agents. Then the 21 tyrosine (Tyr) residues in BSA mainly reduce Au^{III} ions through the phenolic groups.[18]

We thus propose that the growth mechanism of insulin–Au NCs differs from that of BSA–Au NCs. One objection to the Au–S linkage being involved in the insulin–Au NCs lies in the fact that there are only six Cys residues, which are all used up in the cross S–S linkage of A and B chains in forming insulin. Instead, interactions between Au NCs and insulin via amino acids such as tyrosine, lysine, aspartic acid, arginine, and tryptophan are more likely, which have been reported to initiate and control the gold nanostructure synthesis.[18] On the one hand, such a bonding strength resulting from polar–polar interaction may be weaker than that of the Au–S linkage. On the other hand, it offers an advantage by providing semi-free flexibility to the insulin frameworks, so that the insulin–Au NCs preserve the bioactivity of the natural insulin (see below).

In yet another approach, we have intentionally scissored the S–S bond that holds two chains of insulin by reduction. For each chain, the -SH site was terminated by an SO_3H functional group to avoid any S–S crosslinking. As a result, both chains failed to produce any emissive Au NCs, as evidenced by the lack of resolution of any detectable fluorescence at >500 nm. Moreover, the Raman spectra reveal an insulin S–S stretching frequency of about 515 cm^{-1}[19] before and after the encapsulation of Au NCs (see Figure S4 in the Supporting Information), thus supporting the intact S–S crosslinking in insulin–Au NCs. We thus propose that growth and encapsulation of Au NCs proceed by interaction with both chains. In other words, the intact insulin entity provides an optimized structure to foster the formation of Au NCs. The supposedly weak interaction between insulin and Au NCs may cause the expulsion of Au NCs from the insulin upon desorption of the matrix in mass spectrometry, thereby resulting in the breakdown of the unprotected Au NCs.

Insulin is known to be facile in forming crystals. The highly ordered protein assembly with nanosized solvent-filled pores makes insulin crystals capable of promoting Au NC formation. We then added $HAuCl_4$ (1 mM) to an aqueous solution containing insulin crystals. During settling for about two days, the colorless insulin crystals turned yellowish-brown with intense red emission upon UV-lamp (366 nm) irradiation. This result indicated that the high solvent content (51%) of insulin crystals provides accessible channels that allow Au^{3+} to diffuse into the crystals, followed by reduction via, for example, Tyr residues. The two-photon red fluorescence images and spectra of the as-prepared insulin–Au NC crystals acquired under a confocal microscope are shown in Figure 2a and b, respectively. The spectral feature is similar to that of Au NCs in solution. Moreover, Au NCs have grown throughout the entire insulin crystal, as supported by the red emission profile, which is independent of the probing depth (see Figure 2b).

Prior to the application of insulin–Au NCs in cells or tissues, the toxicity of the nanoplatform must be considered. In this study, C2C12, a mouse myoblast cell line, was the test candidate for cytotoxicity evaluation. The cellular effect of

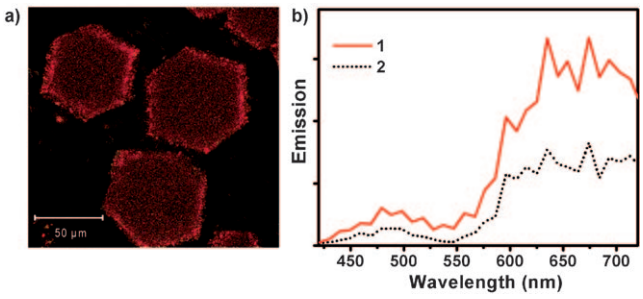

Figure 2. a) Two-photon fluorescence image of insulin–Au NC crystals. The excitation wavelength is 800 nm. b) Emission spectra of different depths of the crystal: 1) on the surface and 2) 5.0 μm below the incident surface.

the insulin–Au NCs, analyzed by MTT assay (MTT = 3-(4,5-dimethylthiazol-2-yl)-2,5-diphenyltetrazolium bromide), for evaluation of cell viability is shown in Figure S5 in the Supporting Information, and demonstrates their superior biocompatibility. We further tested insulin–Au NCs in a more complex matrix, fetal bovine serum (FBS), which contains various growth factors and proteins including BSA, globulins, and fibrinogen. The result in Figure S6 (Supporting Information) shows good stability within at least 2 h.

To ensure internalization between the as-prepared insulin–Au NCs and cells, confocal microscopy and fluorescence staining were utilized. The uptake efficiency of insulin–Au NCs for C2C12 cells may serve as a biomarker to distinguish the differentiated versus undifferentiated C2C12 myoblasts. In a typical protocol, the cells with suitable treatment (see the Supporting Information) were imaged under a confocal microscope to examine the uptake of the insulin–Au NCs after 2 h of feeding. The image obtained was further colorized by color processing to make each compartment more distinguishable. The confocal image depicted in Figure 3 clearly shows that the intense red fluorescence of insulin–Au NCs overlaps with that of the fully differentiated C2C12 mouse myoblasts in the cytoplasm.

To further establish if the particles were internalized by the cells or simply adhered on the surface of the membranes, a detailed two-photon *z*-stacking study was also performed. The results shown in Figure S7b (Supporting Information) confirm that insulin–Au NCs entered into the cell and were distributed in the cytoplasm. In sharp contrast, as evidenced by the weaker red emission, the insulin–Au NC uptake by the undifferentiated C2C12 cells was much smaller. Instead, most insulin–Au NCs remained outside the cell, as confirmed by the fluorescence imaging and *z*-stacking shown in Figure S8 (Supporting Information). The results manifest the insulin receptor overexpression on the differentiated C2C12 cells. We then conducted an inhibition experiment by adding excess insulin to compete with insulin–Au NCs for cellular uptake. The reduction of emission intensity reported by confocal microscopy (see Figure S9 in the Supporting Information) suggests that insulin–Au NCs, in common with insulin, enter cells through receptor-mediated endocytosis; that is, the insulin–Au NCs bind to the insulin receptor and then enter the cell.

While performing internalization experiments, we serendipitously discovered strong X-ray computed tomography (CT) signal elevation in the as-prepared insulin–Au NCs.[20] In this approach, insulin–Au NCs (1–30 mg mL^{-1}) in phosphate-buffered saline (PBS) were tested for CT imaging. The results clearly showed that Au NCs induced a contrast enhancement in a dose-dependent manner (see Figure 4 a). For in vitro tests,

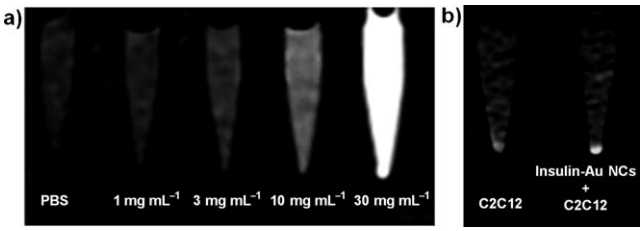

Figure 4. a) CT imaging of insulin–Au NCs in sequential dosage and b) differentiated C2C12 myoblasts with (20 mg mL^{-1}, right) and without (left) insulin–Au NCs.

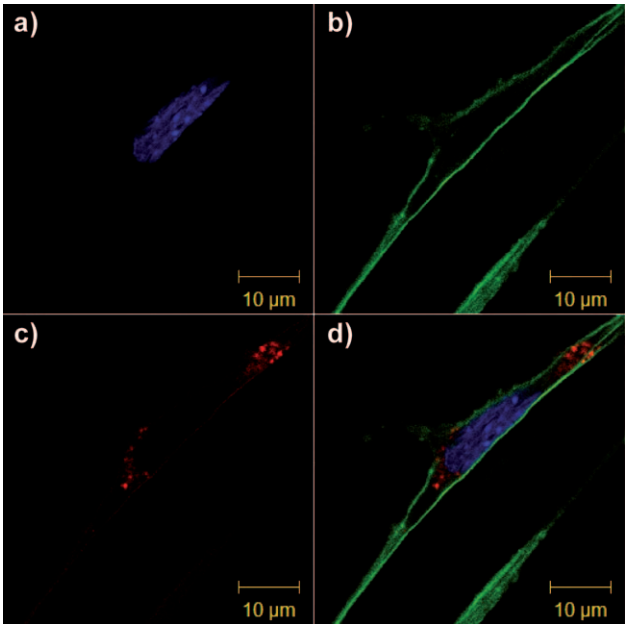

Figure 3. Microscopic observation of internalization of the insulin–Au NCs. Differentiated C2C12 myoblasts were treated with insulin–Au NCs for 2 h. a) Cell nucleus stained with 4′,6-diamidino-2-phenylindole (DAPI, blue). b) Actin fiber stained with Alexa Fluor 488 phalloidin to confirm the cell boundary (green). c) Insulin–Au NCs exhibit red luminescence. d) Fluorescence image overlay of the three images.

differentiated C2C12 myoblasts were treated with insulin–Au NCs and then purified to obtain the cells only for the axial CT slices. As revealed in Figure 4 b, the insulin–Au NCs encapsulated in C2C12 myoblasts showed apparent CT enhancement. Such a contrasting effect demonstrates the insulin–Au NC uptake through endocytosis. The finding of strong CT signal elevation for fluorescent Au NCs may show their potential as a two-in-one agent, that is, for fluorescence and CT imaging.

As a result of the excellent biocompatibility, we then moved one step further toward in vivo testing. Our prime aim was to evaluate the bioactivity of the as-prepared insulin–Au NCs. In this approach, C57BL/6J mice were fed insulin–Au NCs to examine the regulation of glucose level (see the Supporting Information for detailed experimental procedure). The result shown in Figure 5 is both promising and encouraging. It was found that, under the same dosage of 1.0 unit kg^{-1}, an intraperitoneal (i.p.) injection of insulin–Au NCs into anesthetized Wistar rats rendered a trend of reducing the blood glucose similar to that of commercial insulin (Humulin R, see Figure 5). In other words, the blood-glucose-lowering activities of Humulin R and insulin–Au NCs showed no significant difference, which implies that the as-prepared insulin–Au NCs retained bioactivity in reducing blood glucose.

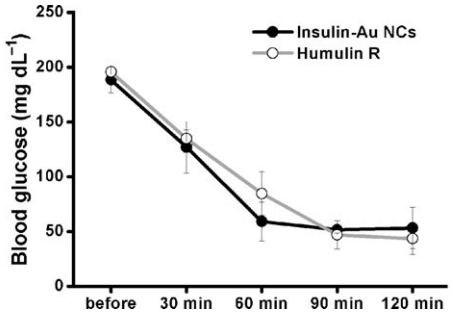

Figure 5. Blood glucose versus elapsed time of treatments with insulin–Au NCs and Humulin R of Wistar rats.

Another crucial experiment was to investigate the metabolism of insulin (that is, insulin–Au NCs), in which insulin-degrading enzyme (IDE) in cytoplasm plays a key role in the proteolytic degradation and inactivation of insulin.[21] In this approach, the IDE-abundant brain homogenate was applied so that the emission properties of the insulin–Au NCs could be investigated in the interaction between IDE and insulin–Au NCs (see below). The results shown in Figure 6 clearly

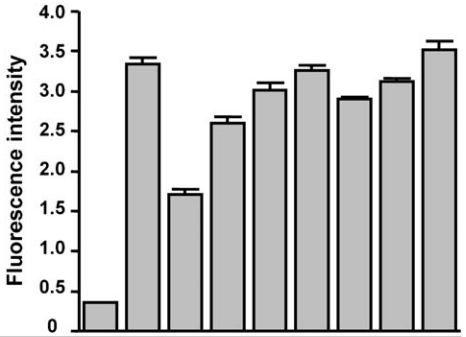

Brain homogenate	+	-	+	+	+	+	+	+	+
Insulin-Au NCs	-	+	+	+	+	+	+	+	+
Racecadotril (mM)	-	-	-	0.01	0.1	1	-	-	-
Thiorphan (mM)	-	-	-	-	-	-	0.01	0.1	1

Figure 6. Fluorescence quenching (monitored at 670 nm) of insulin–Au NCs by brain homogenate and brain homogenate inhibited by racecadotril and thiorphan (see text for details).

indicate that adding insulin–Au NCs to the brain homogenate caused significant quenching (ca. 50%) of the Au NC emission at 670 nm. In yet another experiment, we then treated fresh brain homogenate with racecadotril and thiorphan,[22,23] both of which have been known to inhibit IDE, followed by the addition of insulin–Au NCs. The 670 nm emission intensity was regained and signal recovery was increased upon increasing the racecadotril (or thiorphan) dosage from 0.01 to 1 mM (see Figure 6). The resulting trend indicates that degradation of insulin by IDE may lead to the release of unprotected Au NCs and hence an increase of either the aggregation of Au NCs or the defect sites on the surface of the particles, thereby resulting in the quenching of the emission. Evidence of the former possibility is provided in the TEM measurement, in which large Au NC aggregates are sporadically seen upon addition of IDE to insulin–Au NCs (see Figure S10 in the Supporting Information). The results further confirm that both racecadotril and thiorphan inhibit IDE and hence prevent the degradation of the insulin–Au NCs, thus demonstrating exquisitely that the newly developed insulin–Au NCs are potent in detecting insulin-related biological signals.

In conclusion, we have reported for the first time the insulin-directed synthesis of fluorescent gold NCs. The as-prepared insulin–Au NCs show excellent biocompatibility and retain the insulin bioactivity. Versatility in applications such as fluorescence imaging, CT, and in vivo blood-glucose regulation has been successfully demonstrated. The insulin–Au NC imaging techniques may provide innovative and supplementary methods in addition to conventional isotope ^{125}I-insulin and anti-insulin antibody conjugated to chemiluminescent enzyme, which should be highly attractive to biolabeling and bioimaging applications in the future.

Received: January 13, 2011
Revised: March 23, 2011
Published online: June 17, 2011

Keywords: biomaterials · fluorescence · gold · imaging agents · nanostructures

[1] a) W. Jiang, S. Mardyani, H. Fischer, W. C. W. Chan, *Chem. Mater.* **2006**, *18*, 872–878; b) C.-W. Lai, Y.-H. Wang, Y.-C. Chen, C.-C. Hsieh, B. P. Uttam, J.-K. Hsiao, C.-C. Hsu, P.-T. Chou, *J. Mater. Chem.* **2009**, *19*, 8314–8319.

[2] A. A. Bhirde, V. Patel, J. Gavard, G. Zhang, A. A. Sousa, A. Masedunskas, R. D. Leapman, R. Weigert, J. S. Gutkind, J. F. Rusling, *ACS Nano* **2009**, *3*, 307–316.

[3] J. F. Weng, J. C. Ren, *Curr. Med. Chem.* **2006**, *13*, 897–909.

[4] a) J. M. Abad, L. E. Sendroiu, M. Gass, A. Bleloch, A. J. Mills, D. J. Schiffrin, *J. Am. Chem. Soc.* **2007**, *129*, 12932–12933; b) A. Dass, A. Stevenson, G. R. Dubay, J. B. Tracy, R. W. Murray, *J. Am. Chem. Soc.* **2008**, *130*, 5940–5946; c) S. Link, M. A. El-Sayed, T. G. Schaaff, R. L. Whetten, *Chem. Phys. Lett.* **2002**, *356*, 240–246; d) P. Pyykkö, *Angew. Chem.* **2004**, *116*, 4512–4557; *Angew. Chem. Int. Ed.* **2004**, *43*, 4412–4456; e) G. Schmid, *Angew. Chem.* **2008**, *120*, 3548–3550; *Angew. Chem. Int. Ed.* **2008**, *47*, 3496–3498; f) Z. Liu, L. Peng, K. Yao, *Mater. Lett.* **2006**, *60*, 2362–2365; g) G. H. Woehrle, L. O. Brown, J. E. Hutchison, *J. Am. Chem. Soc.* **2005**, *127*, 2172–2183.

[5] a) M. Eichelbaum, B. E. Schmidt, H. Ibrahim, K. Rademann, *Nanotechnology* **2007**, *18*, 355702; b) P. D. Jadzinsky, G. Calero, C. J. Ackerson, D. A. Bushnell, R. D. Kornberg, *Science* **2007**, *318*, 430–433; c) B. Wahl, L. Kloo, M. Ruck, *Angew. Chem.* **2008**, *120*, 3996–3999; *Angew. Chem. Int. Ed.* **2008**, *47*, 3932–3935; d) N. K. Chaki, Y. Negishi, H. Tsunoyama, Y. Shichibu, T. Tsukuda, *J. Am. Chem. Soc.* **2008**, *130*, 8608–8610; e) D. E. Jiang, M. L. Tiago, W. D. Luo, S. Dai, *J. Am. Chem. Soc.* **2008**, *130*, 2777–2779.

[6] a) C.-C. Huang, Z. Yang, K.-H. Lee, H.-T. Chang, *Angew. Chem.* **2007**, *119*, 6948–6952; *Angew. Chem. Int. Ed.* **2007**, *46*, 6824–6828; b) S. Chen, R. S. Ingram, M. J. Hostetler, J. J. Pietron, R. W. Murray, T. G. Schaaff, J. T. Khoury, M. M. Alvarez, R. L. Whetten, *Science* **1998**, *280*, 2098–2101; c) J. Zheng, R. M. Dickson, *J. Am. Chem. Soc.* **2002**, *124*, 13982–13983; d) H. G. Boyen, G. Kästle, F. Weigl, P. Ziemann, G. Schmid, M. Garnier, P. Oelhafen, *Phys. Rev. Lett.* **2001**, *87*, 276401.

[7] C.-L. Liu, M.-L. Ho, Y.-C. Chen, C.-C. Hsieh, Y.-C. Lin, Y.-H. Wang, M.-J. Yang, H.-S. Duan, B.-S. Chen, J.-F. Lee, J.-K. Hsiao, P.-T. Chou, *J. Phys. Chem. C* **2009**, *113*, 21082 – 21089.
[8] C.-A. J. Lin, T.-Y. Yang, C.-H. Lee, S. H. Huang, R. A. Sperling, M. Zanella, J. K. Li, J.-L. Shen, H.-H. Wang, H.-I. Yeh, W. J. Parak, W. H. Chang, *ACS Nano* **2009**, *3*, 395 – 401.
[9] a) A. Retnakumari, S. Setua, D. Menon, P. Ravindran, H. Muhammed, T. Pradeep, S. Nair, M. Koyakutty, *Nanotechnology* **2010**, *21*, 055103; b) R. Zhou, M. Shi, X. Chen, M. Wang, H. Chen, *Chem. Eur. J.* **2009**, *15*, 4944 – 4951.
[10] J. Xie, Y. Zheng, J. Y. Ying, *J. Am. Chem. Soc.* **2009**, *131*, 888 – 889.
[11] W. Y. Chen, J. Y. Lin, W. J. Chen, L. Y. Luo, E. W. G. Diau, Y. C. Chen, *Nanomedicine* **2010**, *5*, 755 – 764.
[12] a) H. Wei, Z. Wang, L. Yang, S. Tian, C. Hou, Y. Lu, *Analyst* **2010**, *135*, 1406 – 1410; b) J. Xie, Y. Zheng, J. Y. Ying, *Chem. Commun.* **2010**, *46*, 961; c) Y. Liu, K. Ai, X. Cheng, L. Huo, L. Lu, *Adv. Funct. Mater.* **2010**, *20*, 951 – 956.
[13] X. Wu, X. He, K. Wang, C. Xie, B. Zhou, Z. Qing, *Nanoscale* **2010**, *2*, 2244 – 2249.
[14] M. E. Aubin-Tam, W. Hwang, K. Hamad-Schifferli, *Proc. Natl. Acad. Sci. USA* **2009**, *106*, 4095 – 4100.
[15] S. M. de la Monte, J. R. Wands, *J. Alzheimer's Dis.* **2005**, *7*, 45 – 61.
[16] S. E. Kahn, R. L. Hull, K. M. Utzschneider, *Nature* **2006**, *444*, 840 – 846.
[17] M. Tatar, A. Bartke, A. Antebi, *Science* **2003**, *299*, 1346 – 1351.
[18] M. B. Dickerson, K. H. Sandhage, R. R. Naik, *Chem. Rev.* **2008**, *108*, 4935 – 4978.
[19] N. T. Yu, C. S. Liu, D. C. Oshea, *J. Mol. Biol.* **1972**, *70*, 117 – 132.
[20] J. F. Hainfeld, D. N. Slatkin, T. M. Focella, H. M. Smilowitz, *Br. J. Radiol.* **2006**, *79*, 248 – 253.
[21] a) W. C. Duckworth, *Endocr. Rev.* **1998**, *19*, 608 – 624; b) W. Farris, S. Mansourian, Y. Chang, L. Lindsley, E. A. Eckman, M. P. Frosch, C. B. Eckman, R. E. Tanzi, D. J. Selkoe, S. Guenette, *Proc. Natl. Acad. Sci. USA* **2003**, *100*, 4162 – 4167.
[22] H. Wu, C. Chang, K. Cheng, C. Yeh, J. Cheng, *Horm. Metab. Res.* **2010**, *42*, 261 – 267.
[23] a) A. J. Matheson, S. Noble, *Drugs* **2000**, *59*, 829 – 835; b) E. G. Erdos, R. A. Skidgel, *FASEB J.* **1989**, *3*, 145 – 151.

